Optics and Lasers in Engineering 127 (2020) 105978

Contents lists available at ScienceDirect

Optics and Lasers in Engineering

journal homepage: www.elsevier.com/locate/optlaseng

Observation range measuring method based on incoherent digital holographic imaging

Hai Yu*, Jiabin Wu

Changchun Institute of Optics, Fine Mechanics and Physics, Chinese Academy of Sciences, Changchun 130033, China

ARTICLE INFO

Keywords:
Incoherent holography
Phase-shift reconstruction
Observed distance
Ranging measuring

ABSTRACT

An incoherent digital holographic imaging system was constructed in this study based on the Michelson interferometer, where the distance of the observed object can be calculated via mathematical modeling. We obtain the composite hologram by generalized phase-shifting method, then utilize the contrast evaluation function to determine the focus distance of composite hologram. The relationship between the focus distance and observation distance is deduced accordingly to complete the measurement process. Experiments show that the uncertainty of the proposed method decreases as observed distance increases in the range of 508 mm–660.4 mm. The results presented in this paper may provide a theoretical foundation for incoherent holographic imaging and three-dimensional measurement.

1. Introduction

Digital holography technology can be used to obtain light fields of object as per the intensity of interference fringes between object light and reference light, which is of great interest to researchers and engineers [1–8]. Advancements in computer technology have rendered notable developments in holographic technology. Mikuła [9], Wu [10], Pham [11], Sucerquia [12], Rostykus [13], Abbasian [14], Byeon [15], Haglund [16], and other scholars across the globe have made remarkable achievements in digital holographic reconstruction. Traditional holography necessitates recording the interference of reference light and object light, which has a very limited range of application. And coherent light source illumination also introduces noise that markedly affects the image quality [17].

An incoherent holographic technique is proposed which uses the wave characteristics of light to resolve the coherent noise problem. When using incoherent light, the surface of the observed object is regarded as several incoherent point sources. The light waves emitted by each point source change into two self-coherent beams as they pass through the beam-splitter system, then self-interference occurs on the surface of the image sensor.

Incoherent optical holography is a hot topic in the holographic imaging technology field. Kim [18], for example, proposed a full color natural light holographic camera based on the Michelson interferometer. Choi [19] used a geometric-phase hologram lens to realize incoherent holographic imaging. Rai [20] proposed a single camera shot holography technique based on coded aperture correlation; Nobukawa [21] implemented single-shot phase-shifting incoherent digital holography with multiplexed checkerboard phase gratings. Nguyen [22] established an off-axis incoherent holographic recording optical path to separate conjugate images from the original images.

There have been many other valuable contributions to the literature. Katz [23] analyzed the imaging resolution of an incoherent digital holography system. Cai [24] proposed an incoherent digital holographic reconstruction method based on the generalized phase shift. Indeed, studies have shown that self-interference holography allows the user to record the amplitude and phase of observed objects to gather their three-dimensional (3D) information.

The self-interference holographic technique can utilize the phase information of an observed object light wave. This remits several important advantages.

(1) The holographic imaging system works based on a focusing algorithm, thus eliminating the focusing mechanism of the traditional imaging system.
(2) The lateral resolution of self-interference holography can be higher than that of traditional optical imaging systems [25].
(3) Stereo measurement of the observed object can be realized because its phase information is preserved [26].

It is necessary to determine the observed distance of the holographic imaging system in order to achieve stereo measurement with holographic imaging technology. Acquiring the observed distance via imaging method will greatly reduce the complexity of the observation system.

This paper proposes a novel method of measuring observation distance based on incoherent optical digital holographic reconstruction.

* Corresponding author.
E-mail address: yuhai@ciomp.ac.cn (H. Yu).

https://doi.org/10.1016/j.optlaseng.2019.105978
Received 15 August 2019; Received in revised form 28 November 2019; Accepted 2 December 2019
Available online 9 December 2019
0143-8166/© 2019 Elsevier Ltd. All rights reserved.

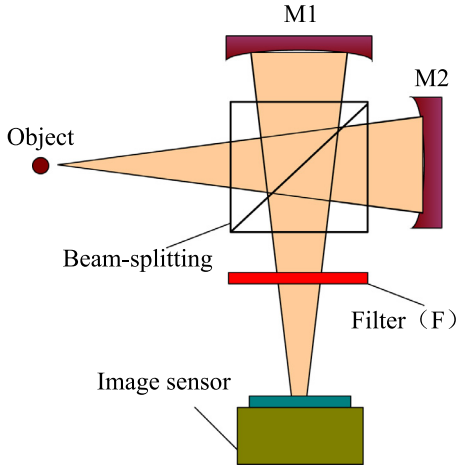

Fig. 1. Self-interference holographic imaging system.

The optical path of the incoherent optical digital hologram is constructed using a Michelson interferometer, then the compound hologram is obtained according to the generalized phase shift. The contrast evaluation function determines the focusing distance of the hologram. Finally, the observed distance model is established and the observed distance obtained by transformation of the model. Experiments show that when an object is fixed at a distance of 508 mm, the ranging uncertainty of the proposed system's observation is 3.31 mm. When the distance between the observed objects ranges from 508 mm to 660.4 mm, the uncertainty is 8.25 mm. The results presented below may provide theoretical support for more sophisticated incoherent optical digital holography measurement techniques.

The remainder of this paper is structured as follows. Section 2 explains the optical path principle and holographic reconstruction method based on incoherent digital holographic imaging technology. Section 3 explains the proposed observed distance measurement method. Section 4 describes the experiment conducted to test the proposed method, and Section 5 provides a brief summary and conclusion.

2. Principles of incoherent holographic imaging

2.1. Holographic recording principle

Similar to Fresnel Incoherent Holography (FINCH), a Michelson interferometer was used in this study to design the optical path of an incoherent digital holographic recording system (Fig. 1).

The system includes the observed object, concave reflector M1 and M2, beam-splitter, filter, and image sensor. The light waves emitted by each point source are divided into two beams by a beam-splitter (1:1). After reflection by concave mirrors M1 and M2, respectively, the beam is combined again and presents self-interference on the surface of the image sensor. The interference fringes are recorded by image sensors to achieve holographic recording.

The propagation function of the light wave is:

$$h(x, y, z) = exp\left[\frac{j\pi}{\lambda z}(x^2 + y^2)\right] \tag{1}$$

The hologram expression recorded by the imaging system in Fig. 1 is:

$$I = C + O^*(x, y, z_h) \otimes h(x, y, z_h) + O(x, y, z_h) \otimes h^*(x, y, z_h) \tag{2}$$

Where "⊗" denotes a convolution operation, C is the DC component, O is the observed object light wave, O^* is the complex conjugation of O, and h^* denotes the complex conjugation of h. z_h is the focusing distance. Eq. (2) contains a conjugate image and DC component, which interfere with the reconstruction, make the image noisy, and do not allow for clear images to be obtained.

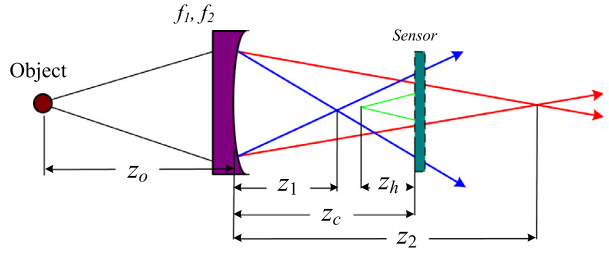

Fig. 2. Optical path coordinate system.

2.2. Generalized phase shift algorithm principle

Removing the conjugate image and DC component are the keys to securing clear wave information. A four-step phase-shifting process was used for reconstruction in this study. When recording holograms, four holograms with different phases were recorded by vibration and other methods: $I1$, $I2$, $I3$, and $I4$, respectively. Assuming the phase difference between $I2$ and $I1$ is α_1, the phase difference between $I3$ and $I2$ is α_2 and the phase difference between $I4$ and $I3$ is α_3. The difference of phase α_1, α_2, and α_3 can be determined by gray value statistics method, the compound hologram can be obtained as follows [24]:

$$O(x, y, z_h) = A\exp(i\phi) = \frac{1}{4\sin(\alpha_1 + \alpha_2)}\left\{\frac{\exp\left[i(\alpha_1 + \alpha_2)/2\right]}{\sin\left[(\alpha_2 + \alpha_3)/2\right]}(I2 - I4) - \frac{\exp\left[i(\alpha_1 + \alpha_2/2 + \alpha_3/2\right]}{\sin\left[(\alpha_1 + \alpha_2)/2\right]}(I1 - I3)\right\} \tag{3}$$

where i is an imaginary unit, A is the amplitude of the composite hologram, and φ is the phase. The composite hologram $O(x, y, z_h)$ in Eq. (3) is an object light wave diffracted by z_h distance. By inverse diffraction of the composite hologram, the information of the in-focus object light wave can be obtained as follows:

$$O(x, y, 0) = O(x, y, z_h) \otimes h^*(x, y, z_h) \tag{4}$$

where z_h is the focusing distance, "⊗"represents the convolution operation, $O(x, y, 0)$ is the in-focus object wave, and h^* is the complex conjugation of h.

As expressed in Eq. (4), accurate judgment of focusing distance is the key to accurate distance measurement. When the hologram is reconstructed by an incorrect focusing distance, the amplitude image will be defocused resulting in a decrease in image contrast. Here, we use the following contrast evaluation function to acquire the focusing distance:

$$F = \frac{1}{MN}\sum_{x}^{M}\sum_{y}^{N}\left[\frac{A(x, y) - \bar{A}}{A(x, y)}\right]^2 \tag{5}$$

Where A denotes the amplitude of the object light and $\bar{A}$denotes the average amplitude. M and N are the ranges of x and y of the hologram, respectively. As the focusing distance z_h changes gradually, the position at which F is maximal becomes the best focusing position and the best focusing distance can be determined accordingly.

3. Calculation of observation distance

3.1. Principle of calculating observation distance

First, we established the coordinate system with the elements of Fig. 1 as shown in Fig. 2.

The focal lengths of the mirrors shown in Fig. 2 are f_1 and f_2, and the imaging distances of the two mirrors are z_1=($z_o f_1$)/(z_o-f_1), z_2=($z_o f_2$)/(z_o-f_2). Next, we set the distance between the image sensor and the mirror as z_c. The focusing distance can be expressed as follows

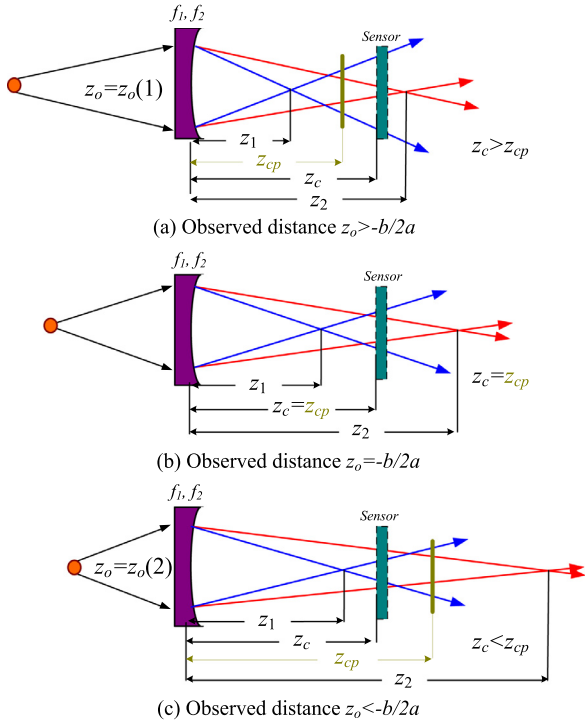

Fig. 3. Principles of light paths at different distances.

[23]:

$$z_h = -\frac{(z_1 - z_c)(z_c - z_2)}{z_1 - z_2} \tag{6}$$

By extrapolating z_1 and z_2 into Eq. (6), we can express z_o as follows:

$$az_o^2 + bz_o + c = 0 \tag{7}$$

where the coefficients of the binary linear equation are:

$$\begin{cases} a = (z_c - f_1)(z_c - f_2) - (f_1 - f_2)z_h \\ b = -\left[z_c^2(f_1 + f_2) - 2f_1 f_2 z_c\right] \\ c = z_c^2 f_1 f_2 \end{cases} \tag{8}$$

Solving Eq. (7) yields the following expression:

$$\begin{cases} z_o(1) = \frac{-b+\sqrt{b^2-4ac}}{2a} \\ z_o(2) = \frac{-b-\sqrt{b^2-4ac}}{2a} \end{cases} \tag{9}$$

Eq. (7) is a quadratic equation, so there are two z_o solutions as shown in Eq. (9). In order to ensure the unique value of z_o, it is necessary to adjust the optical path so that z_o is in a monotonic range.

In Eq. (6), set the expression of z_h is a quadratic function with z_c as its variable. The derivative of z_c can be obtained as follows:

$$\frac{dz_h}{dz_c} = \frac{2z_c - (z_1 + z_2)}{z_1 - z_2} \tag{10}$$

Let $dz_h/dz_c = 0$ and get $z_c = (z_1 + +z_2)/2$, then the focusing distance z_h reaches an extreme value. After introducing $z_c = (z_1 + +z_2)/2$ into Eq. (9), $z_o(1) = z_o(2) -= b/2a$. Here, $z_o(1)$ and $z_o(2)$ correspond to z_c at each side of the $(z_1 + +z_2)/2$ position, respectively. Let $z_{cp}=(z_1+z_2)/2$, so the position of z_c is related to the observed distance z_o as follows.

- When $z_c=z_{cp}$, the observed distance is $z_o=-b/2a$ (Fig. 3(b));
- When $z_{cp}<z_c<z_2$, the observed distance is $z_o>-b/2a$ and the solution of Eq. (7) is $z_o(1)$, as shown in Fig. 3(a);
- When $z_1<z_c<z_{cp}$, the observed distance is $z_o<-b/2a$ and the solution of Eq. (7) is $z_o(2)$, as shown in Fig. 3(c).

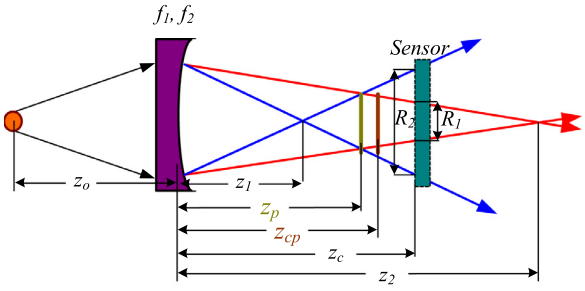

Fig. 4. Imaging resolution optical path principle.

To ensure the monotonicity of the focusing distance, we limited the observed distance $z_o > -b/2a$ to make sure that $z_{cp} < z_c < z_2$. The solution of Eq. (7) is then $z_o = z_o(1)$.

3.2. Uncertainty analysis

According to Eq. (8), the focusing distance of the hologram directly affects the accuracy of the observation distance algorithm. The contrast evaluation algorithm is used to obtain the focusing distance, so the effect of the image resolution on the focusing effect is not negligible.

We set the aperture of the mirrors M1 and M2 as R_M, so the aperture radii of the mirrors M1 and M2 are R_1 and R_2, respectively (Fig. 4). According to the approximate triangle law, the aperture radius of a light wave propagating through M1 and M2 to the image sensor is as follows:

$$R_1 = \frac{z_c - z_1}{z_1} R_M \tag{11}$$

$$R_2 = \frac{z_2 - z_c}{z_2} R_M \tag{12}$$

When the aperture of the reflected light through M1 and M2 mirrors is R_1=R_2, the longitudinal resolution is zero and the lateral resolution is maximal [23]. At this time, the position of the image sensor in the optical path is:

$$z_p = \frac{2z_1 z_2}{z_1 + z_2} \tag{13}$$

The method proposed in this paper is closely related to the vertical resolution of the optical path. When the range of image sensor is set to $z_{cp} < z_c < z_2$, z_c gradually moves away from the z_p position as observed distance z_o increases. At the same time, the vertical resolution of the holographic image gradually increases while the lateral resolution of the holographic image gradually decreases. As a result, the observed distance as-obtained gradually becomes more certain. Within this optical path, the calculations grow more accurate as the observed distance increases.

4. Experiments

4.1. Focus distance experiment

We conducted a series of experiments to verify the validity of the focusing distance determination function on the incoherent hologram. The optical path parameters were set to f_1 = 101.2 mm and f_2 = 152.4 mm. The image sensor was placed at a distance of about z_c = 80 mm from the mirror and the observed object at a distance of about z_o = 254 mm. The range of image acquisition pixels in this case was 512 × 512 pixels, the central wavelength of the filter was 650 nm, and the pixel size was 5.2um. We used a white light LED flashlight to carry out holographic acquisition experiments on irradiated objects. The constructed optical path is shown in Fig. 5 and the collected hologram is shown in Fig. 6.

Fig. 6(a)-(d) shows four holograms with different phases. Fig. 6(e) shows an image of the observed object taken on a mobile phone. Fig. 6(f)

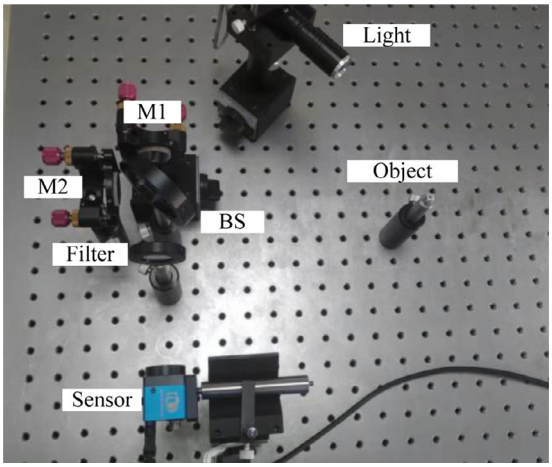

Fig. 5. Experimental optical path.

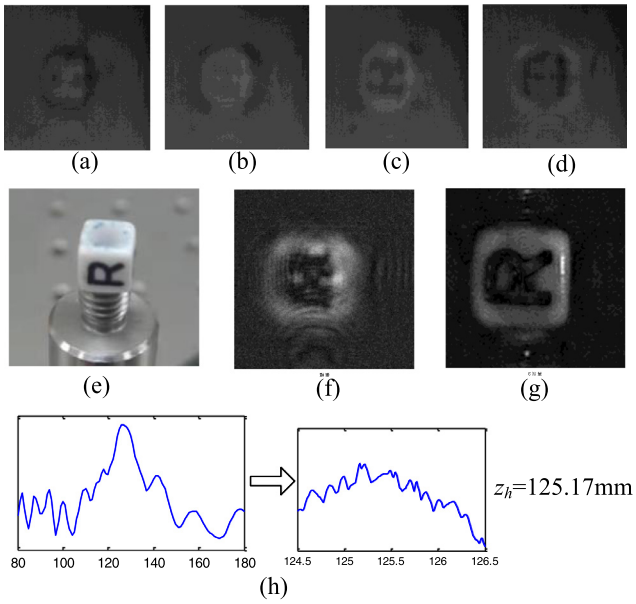

Fig. 6. Holographic recording and focusing distance acquisition.

is a composite hologram with the generalized phase shift algorithm, Fig. 6(g) shows the reconstructed amplitude, and Fig. 6(h) is the result of using the contrast judgment function of Eq. (9). The optimal focusing distance emerges when the curve in Fig. 6(h) reaches its maximum.

4.2. Uncertainty of measurement at uniform distance

We next set the range of image acquisition pixels as 300 × 300 pixels. The range of the observed distance was z_o = 508 mm to 660.4 mm and the position of the image sensor was z_c = 177.8 mm in this case. The resulting light path is shown in Fig. 7. The parameters in the optical path are as follows:

$z_1 = 126.38\,mm \sim 119.51\,mm$;
$z_2 = 217.71\,mm \sim 198.12\,mm$;
$z_{cp} = 172.05\,mm \sim 158.82\,mm$.

According to the above parameters, the coefficients of Eq. (8) are as follows:

$a = 3.23088 \times 10^3$;
$b = -2.5236 \times 10^6$;
$c = 4.8949 \times 10^8$.

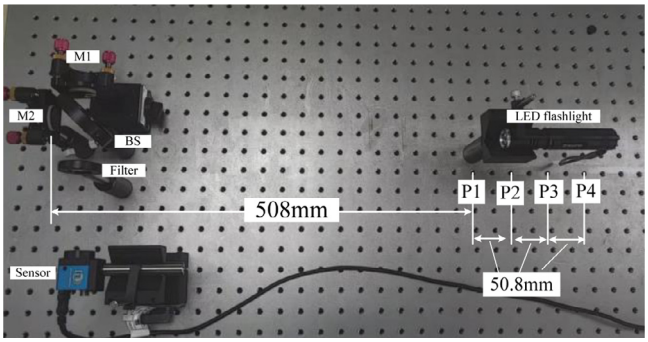

Fig. 7. Principle diagram of multiple acquisition experiments.

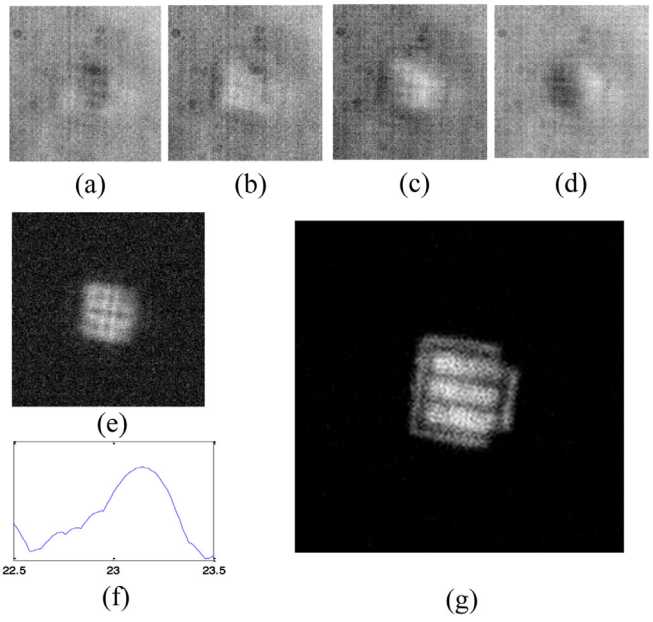

Fig. 8. Holographic recording and reconstruction results.

We next used an LED flashlight as the object to be observed. We placed it at the *P*1 position shown in Fig. 7 (z_o = 508 mm) and collected four images as shown in Fig. 8(a)–(d).

We calculated the generalized phase shift to obtain the composite hologram shown in Fig. 8(e). Fig. 8(f) shows a contrast curve obtained by the contrast evaluation method, where we used a focusing distance of 23.15 mm. Fig. 8(g) shows the reconstruction amplitude. By calculation, when z_h = 23.15 mm, an obverted distance $z_o(1)$ = 493.11 mm was obtained.

To verify the uncertainty, we gathered six hologram recordings when the observed object was at the *P*1 position shown in Fig. 7 (z_o=508 mm). The composite holograms obtained by phase shift operation are shown in Fig. 9(a), the reconstructed amplitudes are shown in Fig. 9(b), and the contrast evaluation function curves are shown in Fig. 9(c). The focusing distances determined according to the contrast evaluation function are shown in Table 1.

As per Eq. (7), the disparity between the observed distance and the set distance (z_o = 508 mm) is as shown in Table 1. We used the standard deviation to assess the uncertainty of $|\mu|$ at the same position, δ_1 = 3.31 mm.

4.3. Measurement uncertainty of different distance intervals

We next moved the observed objects and collected holograms every 50.8 mm. Fig. 10(a)–(d) shows the positions of the LED at *P*1, *P*2, *P*3,

Table 1
Same-distance tests (Unit: mm).

No.	Set distance	Focusing distance (z_h)	Calculated observation distance (z_o)	Differences from set distance ($\|\mu\|$)
1	508	23.15	493.11	14.89
2	508	23.53	484.47	23.53
3	508	23.46	486.08	21.92
4	508	23.54	484.24	23.76
5	508	23.50	485.16	22.84
6	508	23.44	486.54	21.46

Table 2
Different distance tests (Unit: mm).

No.	Set distance	Focusing distance (z_h)	Calculated observation distance (z_o)	Differences from set distance ($\|\mu\|$)
1	508	23.53	485.16	22.84
2	558.8	20.59	547.28	11.52
3	609.6	17.05	619.17	9.57
4	660.4	15.21	657.38	3.02

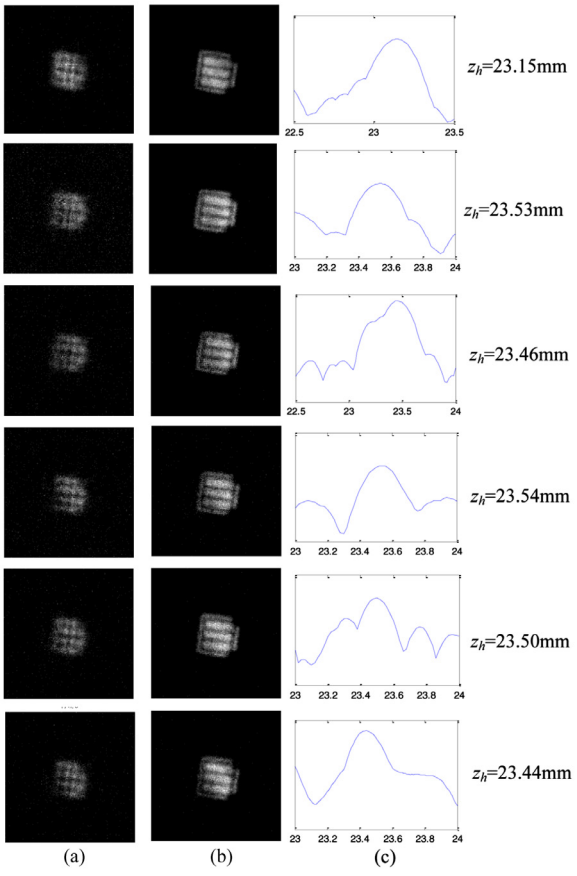

Fig. 9. Multiple imaging results at same location.

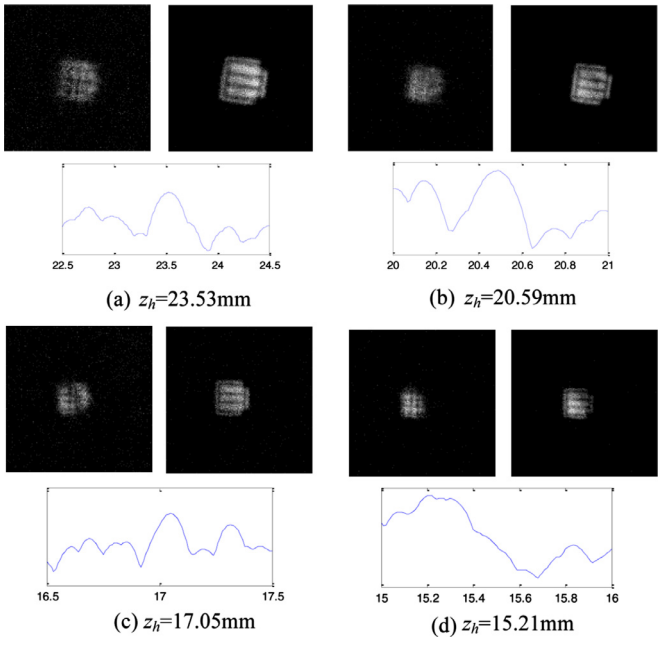

Fig. 10. Holographic recording and reconstruction at different distances.

and *P*4 corresponding to 508 mm, 558.8 mm, 609.6 mm, and 660.4 mm, respectively.

The focusing distance was determined according to Eq. (5) as shown in Table 2. Converted observation distances are listed in the fourth column of the table. The errors between the measured value and the actual value are shown in the fifth column of the table. The standard deviation of the errors is $\delta_2 = 8.25$ mm.

We found that error decreased as the distance of the observed object increased. This suggests that as the observed distance increases, the position of the image sensor z_c moves farther away from z_{cp} and the resolution of the image amplitude decreases, which deteriorate the focusing distance accuracy as-determined via contrast recognition algorithm and increases the measurement error.

The uncertainty of the observation distance calculation system used in this experiment is $\sqrt{\delta_1^2 + \delta_2^2} = 8.89$ mm.

4.4. Experimental analysis

We found that the measurement uncertainty of the proposed method is 3.31 mm for observed objects at the same distance and 8.25 mm for different distances. The main factors causing errors are as follows.

(1) Generalized phase-shift reconstruction technology based on gray-scale statistics leads to some error in hologram reconstruction, i.e., the hologram may contain some noise that influences the measurements.
(2) Error also may emerge when using the contrast method to determine the focusing distance due to noise. This may render the observation distance calculation result inaccurate.

(3) When the distance of the object changes, the relative position of the image sensor in the optical path also changes as does the corresponding imaging resolution. The observation distance calculation accuracy decreases as longitudinal resolution decreases.
(4) Errors caused by inaccurate placement of components in the optical path can also affect the system.

We suggest the following improvements to improve the distance calculation accuracy.

(1) Accurate calculation of composite holograms in the phase-shifting algorithm ensures the clarity of reconstructed holograms.
(2) An accurate focusing distance acquisition algorithm must be deployed to ensure accurate focusing distance information.
(3) The optical path must be adjusted to ensure the effective resolution of the holographic imaging system.
(4) Each component must be placed correctly in the optical path to calibrate the measured data and compensate for any measurement error.

5. Conclusion

Incoherent holography is a type of imaging technology that notably differs from traditional optical imaging technology. Interference fringes of the observed light are recorded and the phase information of the light is retained so that 3D measurement of the observed object can be realized effectively. This technology, which can realize the holographic imaging of objects under solar illumination, has important research value.

The optical path of an incoherent optical digital hologram recorded by Michelson interferometer was analyzed in this study and reconstructed using a four-step phase-shifting method. By establishing a reconstruction model of the holographic recording, the observed distance was deduced in a series of experiments. The method presented in this paper may provide a workable basis for future incoherent optical digital holographic measurement techniques.

Author statement

All the work in this paper including writing, experiment and editing was done by Hai Yu.

Declaration of Competing Interest

None.

Acknowledgment

Thanks to Jiabin Wu for his help in the paper creation process. The innovation point discussion and optical path debugging were jointly completed by Jiabin Wu and Hai Yu. The paper writing and experiments were completed by Hai Yui.

Funding

This project is supported by the National Natural Science Foundation of China (Grant No. 51605465) and the Science and Technology Development Programme of Jilin Province(Grant No. 20180520184JH).

References

[1] Bianco V, Memmolo P, Leo M, et al. Strategies for reducing speckle noise in digital holography. Light Sci Appl 2018;7(48).
[2] Rivenson Y, Zhang Y, Günaydın H. Phase recovery and holographic image reconstruction using deep learning in neural networks. Light Sci Appl 2018;7(17141).
[3] Zhao R, Sain B, Wei Q, et al. Multichannel vectorial holographic display and encryption.. Light Sci Appl 2018;7(95).
[4] Wu Y, Luo Y, Chaudhari G, Calis A, et al. Bright-field holography: cross-modality deep learning enables snapshot 3D imaging with bright-field contrast using a single hologram. Light Sci Appl 2019;8(25).
[5] Sobieranski AC, Inci F, Tekin HC, Yuksekkaya M, Comunello E, Cobra D, et al. Portable lensless wide-field microscopy imaging platform based on digital inline holography and multi-frame pixel super-resolution. Light Sci Appl 2015;5:e346.
[6] Běhal J. Quantitative phase imaging incommon-path cross-referencedholographic microscopy usingdouble-exposure method. Light Sci Appl 2019;9:9801.
[7] Ballard ZS, Zhang Y, Ozcan A. Off-axis holography and micro-optics improve lab-on-a-chip imaging. Light Sci 2017;6:e17105.
[8] Bianco V, Memmolo P, Paturzo M, et al. Quasi noise-free digital holography. Light Sci 2016;5:e16142.
[9] Mikuła M, Kozacki T, Józwik M, Kostencka J. Accurate shape measurement of focusing microstructures in Fourier digital holographic microscopy. Appl Opt 2018;57(1):A197–204.
[10] Wu Y, Ozcan A. Lensless digital holographic microscopy and its applications in biomedicine and environmental monitoring. Methods 2018;136:4–16.
[11] Pham QD, Hayasaki Y. Combining phase images measured in the radiofrequency and the optical frequency ranges. Opt Lett 2017;42(11):2062–5.
[12] Sucerquia JG. Color digital lensless holographic microscopy: laser versus LED illumination. Appl Opt 2016;55(24):6649–54.
[13] Rostykus M, Soulez F, Unser M, Moser C. Compact in-line lensfree digital holographic microscope. Methods 2018;136:17–23.
[14] Abbasian V, Akhlaghi EA, Charsooghi MA, et al. Digital holographic microscopy for 3D surface characterization of polymeric nanocomposites. Ultramicroscopy 2018;185:72–80.
[15] Byeon H, Go T, Lee SJ. Digital stereo-holographic microscopy for studying three-dimensional particle dynamics. Opt Lasers Eng 2018;105:6–13.
[16] Haglund P, Frostevar J, Powell J, et al. Holographic measurement of distortion during laser melting: additive distortion from overlapping pulses. Opt Laser Technol 2018;100:1–6.
[17] Gabor D. A new microscope principle. Nature 1948;161:777–8.
[18] Kim MK. Full color natural holographic camera. Opt Express 2013;21(8):9636–42.
[19] Choi K, Yim J, Yoo S, Min S. Self-interference digital holographywith a geometric-phase hologram lens. Opt Lett 2017;42(19):3940–3.
[20] Rai MR, Vijayakumar A, Rosen J. Single camera shot interferenceless coded aperture correlation holography. Opt Lett 2017;42(19):3992–5.
[21] Nobukawa T, Muroi T, Katano Y, Kinoshita N, Ishii N. Single-shot phase-shifting incoherent digital holography with multiplexed checkerboard phase gratings. Opt Lett 2018;43(8):1698–701.
[22] Nguyen CM, Muhammad D, Kwon HS. Spatially incoherent common-path off-axis color digital holography. Appl Opt 2018;57(6):1504–9.
[23] Katz B, Rosen J, Kelner R, et al. Enhanced resolution and throughput of Fresnel incoherent correlation holography using dual diffractive lenses on a SLM. Opt Express 2012;20(8):9109–21.
[24] Cai LZ, Liu Q, Yang XL. Generalized phase-shifting interferometry with arbitrary unknown phase steps for diffraction objects. Opt Lett 2004;29(2):183–5.
[25] Kim S-G, Lee B, Kim E-S, Yi C-W. Resolution analysis of incoherent triangular holography. Appl Opt 2001;40(26):4672–8.
[26] Wu Y, Cheng HB, Wen YF. High-precision rotation angle measurement method based on a lensless digital holographic microscope. Appl Opt 2018;57:112–18.